

Adjustable Graphene/Polyolefin Elastomer Epsilon-near-zero Metamaterials at Radiofrequency Range

Ji Dai, Hongchun Luo, Mark Gerard Moloney, and Jun Qiu

ACS Appl. Mater. Interfaces, **Just Accepted Manuscript** • DOI: 10.1021/acsami.0c02979 • Publication Date (Web): 21 Apr 2020

Downloaded from pubs.acs.org on April 25, 2020

Just Accepted

"Just Accepted" manuscripts have been peer-reviewed and accepted for publication. They are posted online prior to technical editing, formatting for publication and author proofing. The American Chemical Society provides "Just Accepted" as a service to the research community to expedite the dissemination of scientific material as soon as possible after acceptance. "Just Accepted" manuscripts appear in full in PDF format accompanied by an HTML abstract. "Just Accepted" manuscripts have been fully peer reviewed, but should not be considered the official version of record. They are citable by the Digital Object Identifier (DOI®). "Just Accepted" is an optional service offered to authors. Therefore, the "Just Accepted" Web site may not include all articles that will be published in the journal. After a manuscript is technically edited and formatted, it will be removed from the "Just Accepted" Web site and published as an ASAP article. Note that technical editing may introduce minor changes to the manuscript text and/or graphics which could affect content, and all legal disclaimers and ethical guidelines that apply to the journal pertain. ACS cannot be held responsible for errors or consequences arising from the use of information contained in these "Just Accepted" manuscripts.

Adjustable Graphene/Polyolefin Elastomer Epsilon-near-zero Metamaterials at Radiofrequency Range

Ji Dai ^a, Hongchun Luo ^a, Mark Moloney ^b, Jun Qiu ^{a, c, *}

J. Dai, H. Luo, J. Qiu

^a School of Materials Science and Engineering, Tongji University, Shanghai, 201804, PR China

M. Moloney

^b Department of Chemistry, University of Oxford, 12 Mansfield Road, Oxford, OX1 3TA, England

J. Qiu

^{a, c} Key Laboratory of Advanced Civil Engineering Materials (Tongji University), Education of Ministry, Shanghai, 201804, PR China

E-mail: qiu jun@tongji.edu.cn

Abstract

While epsilon-near-zero (ENZ) metamaterials have marvelously shown various application prospects, the way to construct intrinsic ENZ metamaterials and adjust their ENZ properties precisely are still uncovered. The realization of stable and broadband ENZ properties at the radiofrequency range is of great significance. Herein graphene/polyolefin elastomer (POE) intrinsic ENZ metamaterials are initially constructed via the nanohybrid process. The metamaterials possess excellent adjustable ENZ properties by adjusting the content and reduction methods of graphene. The permittivities maintain between -1 and 1 steadily with increasing graphene content, which is attributed to the moderated carrier concentration of the conductive networks in the nanohybrids. Besides, different reduction methods also have significant impacts on ENZ properties. The hydrazine hydrate reduction method increases the maximum ENZ frequency region to 126MHz. Lorentz type resonance is reasonable for the positive-negative transition in the ENZ frequency regions. As a significant indicator of the emergence of ENZ property, the sudden peak of dielectric loss tangent is observed. This work offers novel routes to construct intrinsic ENZ metamaterials with excellent adjustability in both value of permittivity and ENZ frequency regions.

Keywords: Epsilon-near-zero, intrinsic metamaterials, graphene, adjustability, radiofrequency

1. Introduction

Epsilon-near-zero (ENZ) metamaterials^{1,2} derive from electromagnetic metamaterials. Metamaterials refer to artificial composite structures whose electromagnetic parameters are negative. As unprecedented specific materials, metamaterials have drawn great attention for their remarkable properties in the past few decades.^{3–6} ENZ metamaterials mean a class of materials whose permittivity close to zero over a specific frequency range, the ENZ region with permittivity within -1 and + 1 can be regarded as an important indicator.^{7,8} When the permittivity vanishes, metamaterials with near-zero permittivity can have broad prospects in tunneling of electromagnetic (EM) energy,⁹ energy squeezing,¹⁰ optical switch,¹¹ electromagnetic absorption.¹² For example, a 2D ENZ material can successfully tunnel electromagnetic energy through subwavelength channels and bends.¹³ The energy squeezing and tunneling effect when electromagnetic waves pass through ENZ narrow waveguide channel were confirmed experimentally.¹⁴ Further, ENZ metamaterials exhibit intriguing applications in controlling the nonlinear dynamics.¹⁵ At present, there are a large number of experimental designs using ENZ materials to achieve the desired functions.^{16–18}

Until now, many technical methods based on structural metamaterials have been applied to the preparation of ENZ metamaterials: alternating layers of dielectric and metal,¹⁹ designing periodic unit cells,^{10,20} embedding suitable inclusions in a host medium (Photonic doping),² transparent conducting oxides²¹ and so on. However, these ENZ metamaterials with delicate periodic microstructure are complex in preparation. Furthermore, the applications of structural metamaterials are easily limited by the tremendous plasma frequency of the material itself.¹⁹ It should be noted that it is possible to achieve permittivity close to or slightly less than zero without resorting to the above ways,^{22,23} but the realized ENZ frequency region is narrow and hard to adjust. It is a challenge to achieve adjustable broadband ENZ property by the above methods at radiofrequency.

Intrinsic metamaterials (also known as random metamaterials, which are derived from nanocomposites) have also been proven to realize the similar electromagnetic properties as structural metamaterials. Albeit massive efforts have been conducted related to intrinsic metamaterials, there

are few implementations of ENZ properties based on intrinsic metamaterials. Especially, considering the huge practical value at radiofrequency^{14,24,25}, it is really significant to construct ENZ intrinsic metamaterials. Realizing intrinsic ENZ properties with broadband adjustability will stimulate the development of zero-index metamaterials and promote the research on the control of electromagnetic parameters.

Compared with metals, the moderate charge carrier concentration in conductive networks formed by carbon materials is promising for better ENZ properties. In recent years, carbon-based nanocomposites can show tunable properties in permittivity.^{26–30} Yao et al. achieved carbon nanotubes/polyaniline composites with metamaterial properties.³⁰ Luo used carbon nanotubes and epoxy resin to realize adjustable negative permittivity.³¹ Recently, weakly negative permittivity have been achieved through different carbon structures.^{26,32–34} At the plasma frequency, the permittivity of these metamaterials reaches zero. Current research on tunable permittivity focus on large-magnitude adjustments. For example, the absolute value of the negative permittivity is adjusted from an enormous value to zero abruptly. There are few reports of permittivity with an absolute value less than 1.

With excellent mechanical properties, polyolefin elastomer (POE) can effectively improve the overall mechanical and anti-corrosion capabilities and make the composites elastic.³⁵ Researches related to graphene and its aerogel have aroused great interests due to its remarkable performances in sound, light, electric, magnet and heat and so on.^{28,36–39} Nanocomposites have better performance in thermal, electrical, mechanical performances when using graphene as fillers. Compared to metals, the lower free carrier concentration in graphene is more beneficial to form a weakly negative permittivity property. Therefore, graphene can be regarded as a good candidate for ENZ metamaterials with adjustable permittivity varying between -1 and +1.^{7,8}

In this paper, we combined graphene and polymer to construct ENZ metamaterials. The experimental realization of broadband intrinsic ENZ metamaterials are prepared initially via a nanohybrid process. As an insulating polymer matrix, POE was compounded with graphene. By

adjusting the graphene content and changing the preparation methods of graphene, the adjustability of the ENZ properties is further investigated. The permittivities of metamaterials are tunable to zero successfully and remain stable between -1 and +1 in the broadband region. This study will provide a broad perspective for the design of intrinsic ENZ metamaterials, which can be applied to cloak,¹⁸ sensor^{40,41} and manipulate the flow of heat.⁴²

2. Materials and Methods

2.1 Materials

Polyolefin Elastomer (POE, particle diameter = 0.178 mm) was commercially supplied by the Mitsui Chemicals Group. The hydrazine hydrate, ammonia, toluene, and graphite were purchased from Sinopharm Chemical Reagent Company. All the chemicals were used as-received without any further treatment.

2.2 Preparation of STrGO/POE and HHrGO/POE metamaterials

Graphene oxide (GO) was prepared by the modified Hummers method. Graphite oxide (1g) was dissolved in deionized water (100mL), and ammonia was added dropwise to keep the solution alkaline. After stirring mechanically, the solution was further ultrasonically dispersed for 2h to obtain the GO dispersion. The homogeneous GO dispersion was transferred into a 100 mL Teflon lining reactor. The reactor was assembled in an oven and reacted at 180 °C for 12 h. The resulting cylindrical hydrogel was poured into a low-temperature freezer and pre-frozen. A reduced GO named as STrGO was achieved after being freeze-dried for 72 h and ground. POE particles were impregnated with toluene, when the POE pellets were into a soft gel state, the corresponding mass of graphene powder was added. After extra toluene was vaporized under stirring, the POE coated with STrGO (STrGO/POE) was obtained. The mixed powder was placed in a cylindrical mold to obtain the sample with a diameter of 20 mm and a thickness of 3 mm. The conductive silver paste was applied on the upper and lower ends of the sample and vacuum-dried at 40°C for 24h. The STrGO/POE metamaterials with 40wt%, 50wt%, 60wt% and 70wt% of STrGO are respectively recorded as STrGO/POE-40, STrGO/POE-50, STrGO/POE-60 and STrGO/POE-70.

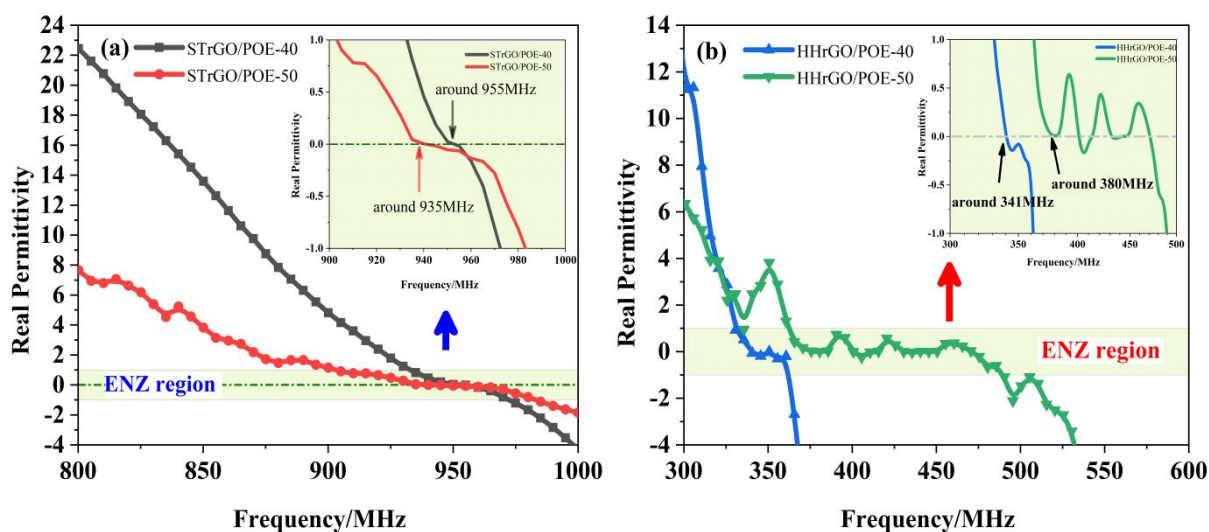
The above homogeneous GO dispersion was mixed with hydrazine hydrate (0.7 g) as reductant under stirring, the reduction reaction would carry out by putting the solution into a flask that was placed in a thermostatic oil bath at 95°C and refluxed for 8h. The product was separated by filtration, washed with distilled water and ethanol, and then vacuum freeze-dried (named as HHrGO). The HHrGO/POE with 20wt%, 30wt%, 40wt%, 50wt% HHrGO were prepared through the same steps with the STrGO/POE metamaterials, and they were recorded as HHrGO/POE-20, HHrGO/POE-30, HHrGO/POE-40 and HHrGO/POE-50.

2.3 Characterization

The dielectric parameters of the metamaterials were measured by Agilent E4991 Precision Impedance Analyzer equipped with a dielectric test fixture (Agilent,16453A) under an AC current of 2 mA in the frequency range of 1MHz-1GHz. The circular samples for dielectric properties were prepared with the diameter of 20mm and thickness of 3 mm. AC electrical resistivity was tested by an electrochemical work station CHI660E. The samples used to test resistivity were the same as the ones for dielectric properties test. The morphology of samples was investigated with scanning electron microscopy (SEM, Quanta FEG200).

3. Results and Discussion

3.1 Realization of ENZ properties in STrGO/POE and HHrGO/POE metamaterials



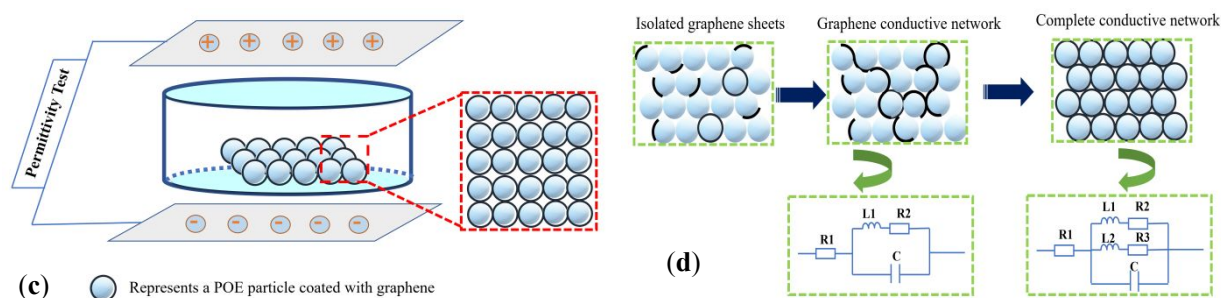


Figure 1. ENZ properties realized in intrinsic metamaterials at radiofrequency (a) STrGO/POE metamaterials; (b) HHrGO/POE metamaterials; (c) Schematic of the sample in the test system; (d) Schematic of the conductive networks at the positive-to-negative transition frequency

The broadband ENZ properties of graphene/POE composites were successfully realized in different radiofrequency regions (**Figure 1**). Obviously, the ENZ properties of this composite could be easily adjusted through changing the graphene content and preparation process. The ENZ property of the STrGO/POE metamaterials is shown in Figure 1(a). It can be seen from the green area (ENZ region) in Figure 1(a) that the permittivity of STrGO/POE-40 is between -1 and +1 at 935MHz-975MHz, and its ENZ region is 40MHz. While STrGO/POE-50 achieves the similar ENZ properties between 905-985MHz, and its ENZ region is 80MHz, more extensive than that of STrGO/POE-40. It is worth noting that the permittivity of STrGO/POE-40 at 945-960MHz is frequency independent, while weak negative permittivity is observed in the composite at a higher frequency. It occurs when the content of the conductive filler added to the insulating matrix exceeds the percolation threshold.⁴³ Further, STrGO/POE-50 further extends this frequency-independent ENZ region to 935-965MHz. This result illustrates that ENZ metamaterials with permittivity between -1 and +1 can be constructed through the insulating polymer matrix and graphene, the magnitude of near-zero permittivity is small and controllable.

The ENZ property of HHrGO/POE is shown in Figure 1(b). When the graphene content is 40wt% (HHrGO/POE-40), the ENZ region obtained is 331-361 MHz (30MHz). The permittivity passes through zero at 341 MHz, and a positive-to-negative transition occurs. It means a dielectric resonance appears in the metamaterial before 340MHz based on Lorentz model.^{32,44} This Lorentz type resonance

should result from the transition of induced electric dipole in the isolated graphene. The positive-to-negative transition shown in Figure 1 could be explained by:

$$\epsilon' = 1 + \frac{\omega_p^2(\omega_0^2 - \omega^2)}{(\omega_0^2 - \omega^2)^2 + \omega^2 T_L^2}$$

where ω , ω_p , ω_0 , T_L respectively means the angular frequency of the applied electric field, angular plasma frequency, resonance frequency, damping parameter in the system. As shown in Figure 1(c), our intrinsic metamaterials are nanohybrids composed of POE and graphene. The upper and lower surfaces of the sample are in an external electric field during the permittivity test. When the AC electric field frequency reaches the characteristic frequency of the composites, the positive-to-negative transition is observed.

When the graphene content of the composite material has not reached the percolation threshold, the isolated graphene coated in the insulating matrix fails to form sufficient contact, which leads to Lorentz type resonance. Besides, HHrGO/POE-50 represents a different trend that its ENZ frequency region becomes wider in 365-491MHz than other metamaterials above , proving that the metamaterials have achieved a wider ENZ frequency region (126MHz) using the reduction graphene with hydrazine hydrate. The reason for stable ENZ properties is related to the conductive structure composed of graphene in the matrix, which is as shown in Figure 1(d). As the graphene content increases, the graphene dispersed in the insulating matrix gradually forms an active connection, so that the carrier density of the entire material is moderate. And the permittivity will shift from capacitive to inductive, resulting in the observed weak negative permittivity. At the same time, due to the high mobility of graphene, stable ENZ properties are formed in metamaterials.

Different ENZ frequency regions are realized, and they can be adjusted by graphene content and reduction method. The obtained ENZ properties are quite different from the other studies, which are based on optical frequency (such as infrared frequency¹¹ and visible light frequency¹⁹). Metamaterials based on insulating POE can exhibit various ENZ properties at different radiofrequency regions. As can be seen from both Figure 1(a) and Figure 1(b), the increasing content of graphene contributes to

the formation of a more stable ENZ property. Compared to Figure 1(a), the positive-to-negative transitions in Figure 1(b) appear in the low frequency regions.

3.2 Adjustability of ENZ regions in STrGO/POE and HHrGO/POE metamaterials based on controlling component content

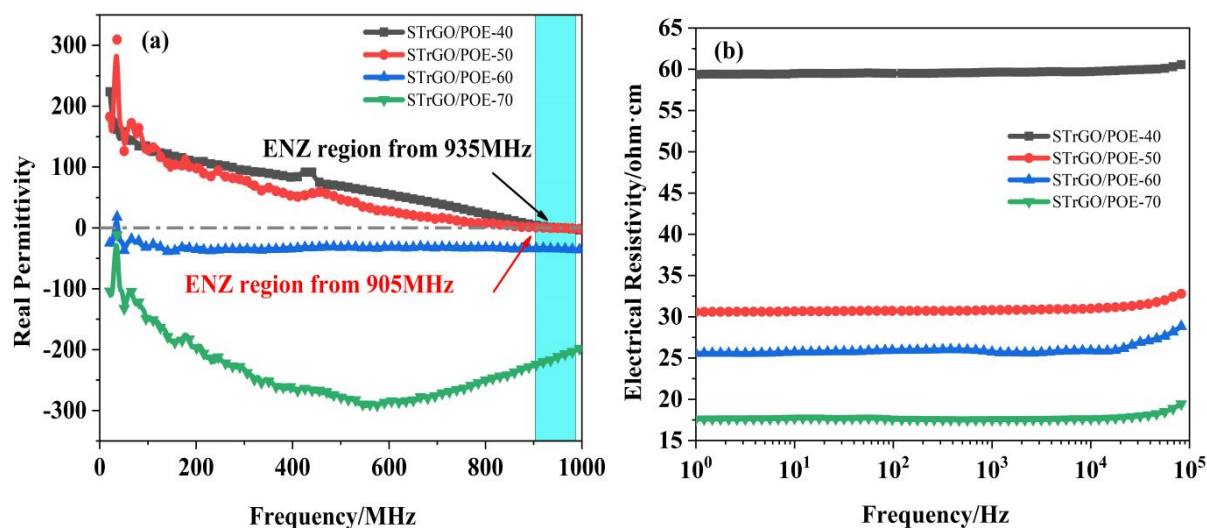


Figure 2. (a) Real permittivity of STrGO/POE metamaterials as a function of frequency; (b) Electrical resistivity of STrGO/POE metamaterials as a function of frequency

The real permittivity of the STrGO/POE metamaterials as a function of frequency is shown in Figure 2(a). The ENZ property emerged at the ultra-high frequency of the radiofrequency region. It can be seen from Figure 2(a) that ENZ properties show apparent dependence on the content of STrGO. For example, negative permittivity was observed in the whole frequency range when 70wt% STrGO was added into the insulating matrix, and its absolute value is enormous. The functional filler already exceeds the percolation threshold inside the composite, which constitutes a series connection according to the Drude model.^{31,45} The inner staggered carbon structure forms a complete conductive network that exhibits properties similar to metals. This result may be related to the Maxwell-Wagner-Sillars effect.³³ The graphene sheets coated with the insulating polyolefin allow electrons to aggregate and form surface polarization under the action of an applied electric field. As the graphene content decreases to 60wt%, the carrier concentration in the metamaterial decreases, which suppresses the increase the magnitude of negative permittivity. The negative permittivity is slightly closer to zero

(between -20 to -30), which is consistent with plasma-like negative permittivity behavior. Interestingly, when the filler content is reduced to 50wt%, the permittivity of the composite occurs unique ENZ property, the near-zero permittivity shows a transition from positive to negative and a frequency-independent region at 935-965MHz. The real permittivity of STrGO/POE-40 also occurs a positive-to-negative transition. More specifically, the real permittivity of STrGO/POE-40 decreases rapidly to 0.81 at 935MHz, while it remains at ± 1 between 935 MHz and 975MHz. By comparison, the composites of STrGO/POE-60 and STrGO/POE-70 with high graphene content now exhibit negative permittivities in the full frequency range.

Meantime, the transition frequency can be changed by adjusting the content of graphene (945MHz in STrGO/POE-40 and 935MHz in STrGO/POE-50). It means the transition frequency shifts forward with the amount of graphene increasing. Moreover, the ENZ frequency region becomes broader with the amount of graphene increasing, the ENZ frequency region in STrGO/POE-40 is 935-975MHz, but it is 905-985MHz in STrGO/POE-50. So, the unique ENZ properties of STrGO/POE metamaterials can be adjusted with the graphene content.

The AC electrical resistivity curves of the above composites at different frequencies are shown in Figure 2(b). As the content of graphene increases, the junction of graphene sheets is further effectively overlapped to form an abundant conductive network, resulting in the decreasing resistivity continuously. The resistivity of STrGO/POE-40 and STrGO/POE-50 are higher than others. This result illustrates that the insufficient carriers in the conductive graphene network are contributed to the ENZ property. Excessive electrical conductivity, however, promotes the transition of composite materials from the Lorentz type to the Drude type.

Figure 3(a) presents the frequency dependences of real permittivity for HHrGO/POE with different HHrGO contents. The near-zero permittivity of the composites is closely related to the amount of HHrGO. When the HHrGO content was 20wt%, the permittivity exceeds 82 in the full frequency range. Because the content of HHrGO in unit volume of the composite was insufficient for enough conductive network, only a large number of micro capacitors were formed. Although the

permittivity decreased rapidly when the graphene content increased to 30wt%, the positive-to-negative transition of the permittivity did not occur within 1M-1GHz. This is because the content of graphene in POE is not enough to form a continuous three-dimensional conductive network at this time. The first positive-to-negative transition occurred at 341MHz in HHrGO/POE-40. When the applied electric field frequency increases to 341MHz, the permittivity of the composite is -0.068. In 331-361MHz, furthermore, the value of permittivity can be maintained within ± 1 . When the graphene content was increased to 50wt%, the permittivity of HHrGO/POE-50 can achieve an ENZ effect in a broader frequency range than that of HHrGO/POE-40. Compared to HHrGO/POE-40, the transition frequency of HHrGO/POE-50 is 366MHz. The ENZ frequency region of HHrGO/POE-50 is 90MHz broader than that of HHrGO/POE-40.

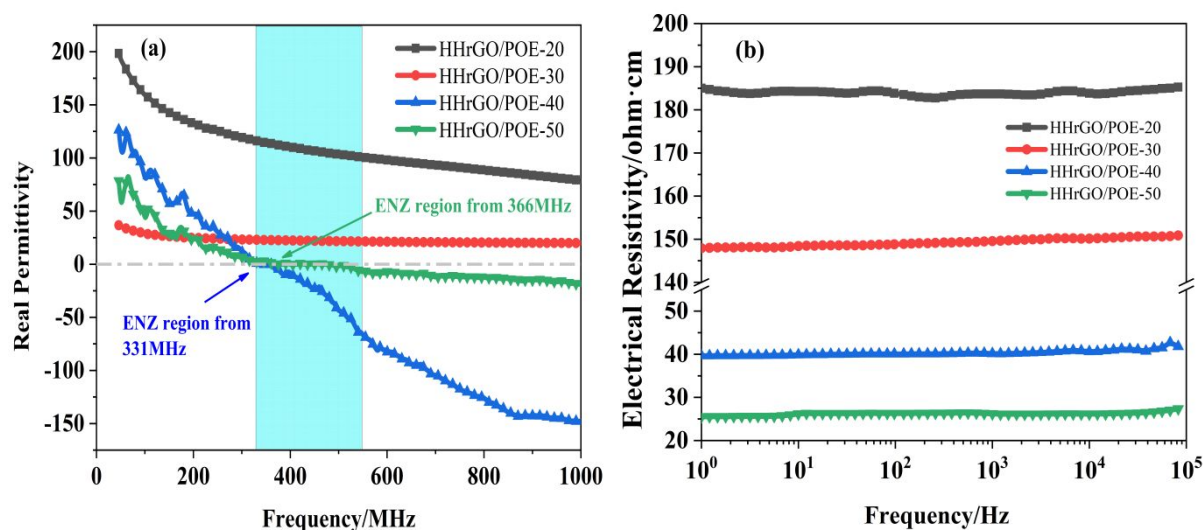


Figure 3. (a) Real permittivity of HHrGO/POE metamaterials as a function of frequency; (b) Electrical resistivity of HHrGO/POE metamaterials as a function of frequency

The electrical resistivity of HHrGO/POE metamaterials are almost independent of frequency as shown in Figure 3(b). The resistivity of composites with graphene content of 20wt% and 30wt% reached 180 $\Omega \cdot \text{cm}$ and 160 $\Omega \cdot \text{cm}$, respectively. When the graphene content does not reach the percolation threshold, the composite exhibits semiconductor properties and its electrical resistivity is high under the action of an external electric field. And the permittivity of the composite shows high and positive in the whole frequency region. When the content of graphene is increased from 30wt%

to 40wt%, the electrical resistivity of the composite drops sharply to $40 \Omega \cdot \text{cm}$. This is consistent with the positive-to-negative transition of permittivity at this content. When graphene content reaches to 50wt%, the resistivity only decreases $14 \Omega \cdot \text{cm}$, which indicates that the three-dimensional conductive network inside the composite has been formed at this time. Under the external electric field, the electron transmission mode has been completed from hopping motion to continuous conduction transition.

Figure 4(a) shows imaginary part of permittivity of STrGO/POE. The imaginary permittivity exhibits a frequency dispersive behavior. That is, the imaginary permittivity drops quickly with frequency increasing before ENZ frequency region. The imaginary permittivity of STrGO/POE-50 is mainly the maximum among the full frequency, the high dielectric loss composite may be used as an efficient electromagnetic wave absorber. The inset in Figure 4(a) shows imaginary part values of STrGO/POE-40 and STrGO/POE-50 in the ENZ frequency regions are close to zero (in line with the real permittivity in Figure 2(a)), and the imaginary part value increases with the increasing of graphene content. The imaginary permittivity ε'' basically derives from conduction loss, dipolar loss, and interfacial polarization loss.

$$\varepsilon'' = \varepsilon_C'' + \varepsilon_D'' + \varepsilon_p'' \quad (1)$$

where ε_C'' is conduction loss, ε_D'' is dipolar loss and ε_p'' is interfacial polarization loss. When the applied electric field frequency is higher than 1MHz, the interface polarization which is from the Maxwell-Wagner effect will disappear.

When graphene content less than 40wt% is added to the insulating POE, the graphene sheets in the obtained composite are difficult to form sufficient conductive networks, so the permittivity loss is mainly dipolar loss. Figure 4(a) shows that the imaginary permittivity of STrGO/POE-40 is lower than other samples. With the increasing content of graphene which is wrapped on the POE, the conductive circuit inside the composite becomes connected. Therefore, the imaginary permittivity is mainly dominated by conduction loss. Conduction loss is usually described by the formula below:

$$\varepsilon_c'' = \frac{\sigma_{dc}}{2\pi f \varepsilon_0} \quad (2)$$

where ε_c'' is conduction loss, σ_{dc} is dc conductivity, ε_0 is vacuum permittivity and f is test frequency. Therefore, the imaginary permittivity decreases sharply as the frequency increases.

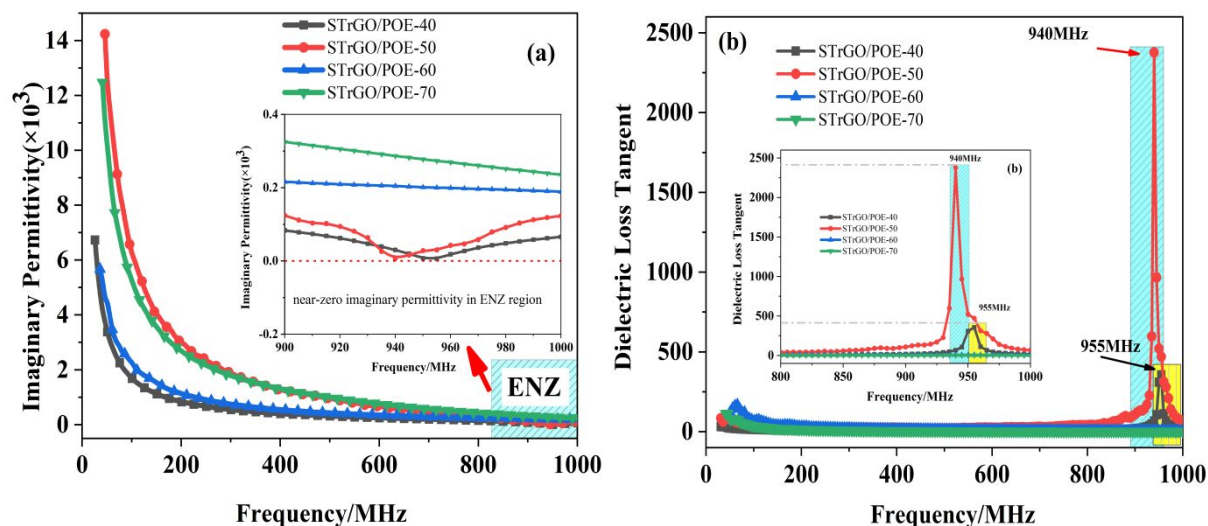


Figure 4. (a) Imaginary permittivity and (b) Dielectric loss tangent ($\tan \delta$) of STrGO/POE metamaterials under different frequency

Figure 4(b) reflects $\tan \delta$ of STrGO/POE as a function of frequency. Compared to the real permittivity of STrGO/POE, it can be seen that a sharp resonance peak appears in the ENZ frequency region, which conforms to the Lorentz model. Especially, a sharp loss resonance peak of STrGO/POE-50 occurs at 940MHz, which 15MHz earlier than that of STrGO/POE-40, and its intensity appears even greater than that of STrGO/POE-40, which corresponds to the results of real permittivity in Figure 2(a). The ENZ property is accompanied by a peak of $\tan \delta$ when a positive-to-negative transition occurs. This is because when the composite changes from the insulating state to the semiconductor state, the internal microcurrent is converged, so that the energy is dissipative in conduction loss at the resonance frequency. When the applied electric field frequency exceeds the resonance frequency, dielectric loss tangent also decreases rapidly due to the weakening of resonance. It is worth noting that when the peak of the dielectric loss tangent appears, the imaginary permittivity of the metamaterials also drops to zero. This result means that the real permittivity and imaginary permittivity of the material are close to zero in the ENZ frequency region simultaneously, which

provides ideas for the ENZ metamaterial without dielectric loss. Meanwhile, the peak of $\tan \delta$ can be used as an important indicator and strong proof of the emergence of ENZ property.

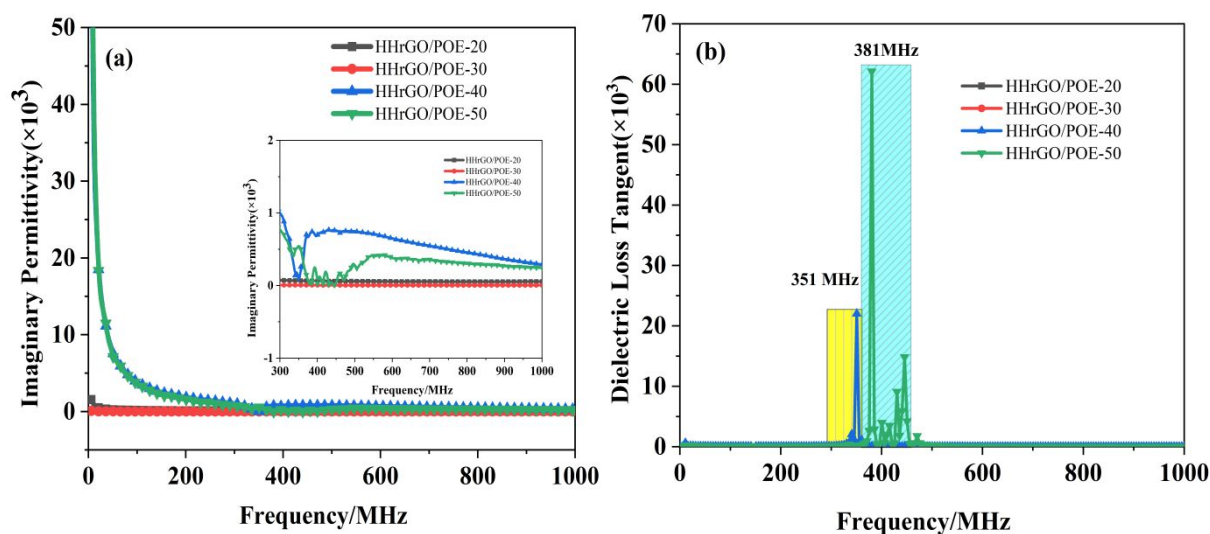


Figure 5. (a) Imaginary permittivity and (b) Dielectric loss tangent ($\tan \delta$) of HHrGO/POE metamaterials under different frequency

Figure 5(a) depicts the imaginary part of permittivity of HHrGO/POE. The imaginary permittivities of HHrGO/POE composites with 20wt% and 30wt% HHrGO tend to be frequency independent. Large imaginary permittivity was observed in HHrGO/POE-40 and HHrGO/POE-50 before ENZ frequency region. The conduction loss in the composites is the main reason for the high imaginary permittivity before 200MHz. Sharp resonance peaks of the dielectric loss tangent also appear in ENZ frequency region, as shown in Figure 5(b). The dielectric loss tangent peak of HHrGO/POE-40 appears at 351MHz, while that of HHrGO/POE-50 is at 380MHz. The imaginary permittivity of the metamaterials also drops to zero at 351MHz and 380MHz. Nevertheless, unlike STrGO-POE, in HHrGO/POE, the peak of dielectric loss tangent of HHrGO/POE-40 appears before that in HHrGO/POE-50. The emergence of $\tan \delta$ proves that the composite prepared first reaches resonance when the graphene content is 40wt%. The sudden peak of the dielectric loss tangent is also observed in polyaniline/multi-walled carbon nanotube nanocomposites.⁴⁶

The results demonstrate that the value of permittivities of STrGO/POE and HHrGO/POE composites can be regulated to near-zero range (-1 to +1) through adjusting the content of graphene.

Meantime, the ENZ frequency region can also effectively regulated near-zero range using different content of graphene for two kinds of metamaterials. As a wider ENZ frequency region emerges in STrGO/POE-50 than in STrGO/POE-40, a similar situation is also found in HHrGO/POE. The ENZ frequency region is 30 MHz in HHrGO/POE-40, and it can be extended to 120 MHz in HHrGO/POE-50. Therefore, adjusting in component content can broad frequency region of ENZ properties. Dielectric loss tangent peak can be used as an effective indicator for generating ENZ property. When $\tan \delta$ peak occurs, the real permittivity and imaginary permittivity of metamaterial are both zero. That is, an ENZ metamaterial with zero loss is successfully constructed.

3.3 Adjustability of ENZ regions of STrGO/POE and HHrGO/POE metamaterials based on preparation process of graphene

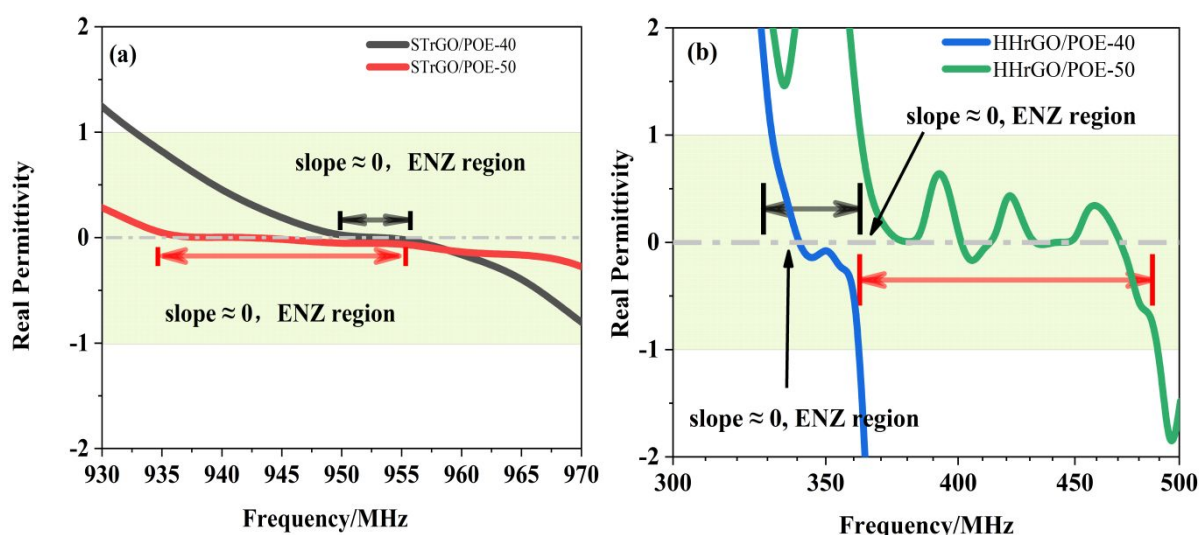


Figure 6. Enlarged views of the frequency region from positive to negative in ENZ metamaterials:

(a) STrGO/POE metamaterials; (b) HHrGO/POE-40 metamaterials

Figure 6 shows that the permittivities of these two types of metamaterials achieve positive-to-negative transitions in corresponding ENZ frequency regions. The transition frequency of STrGO/POE-40 and STrGO/POE-50 are 955MHz and 940MHz, while the transition frequency of HHrGO/POE-40 and HHrGO/POE-50 are 341MHz and 380MHz, respectively. By compared with Figure 6(a) and Figure 6(b), the ENZ property of the STrGO/POE metamaterial appears at around 900-1000MHz. In contrast, the ENZ property of the HHrGO/POE metamaterial is realized at 300-

500MHz. Figure 6(a) shows that the permittivity of STrGO/POE-40 is almost completely close to zero in 950-960MHz, while STrGO/POE-50 extends this result to 935-960MHz. As for HHrGO/POE-40, the permittivity, which is completely close to zero, appears at 341-360MHz, as shown in Figure 6(b). When graphene content reaches 50wt%, the permittivity maintains between 0.42 and -1 at 365-491MHz. The ENZ frequency region of HHrGO/POE-50 expands to 126MHz, which is 46MHz broader than that of STrGO/POE-50. In STrGO/POE composites, Lorentz type resonance appears only once as the frequency increases, while in HHrGO/POE composites, there are multiple positive-to-negative transitions. In the hydrazine hydrate reduction method, the ENZ frequency range shifts forward from 900-1000M to 300-500MHz. The ENZ property realized in different frequency regions is helpful for many applications, such as wireless transmission, bandpass filter. This result provides a new approach to regulate ENZ property of graphene composites.

The reason for the formed different resonance frequencies presented in Figure 6 is the different porosities of the two graphene. Figure 7(a) shows the microstructures of graphene obtained by the solvothermal method. The graphene hydrogel prepared by GO through the solvothermal method has a large porosity, yielding in porous STrGO. Figure 7(b) exhibits the microstructures of graphene obtained by the hydrazine hydrate reduction method. The interlamellar gap of STrGO in Figure 7(a) is more extensive than that of HHrGO in Figure 7(b). Compared with the foam structure of STrGO, the denser HHrGO can be better dispersed in POE, which forms a better conductive carbon network. The microstructures of the composites are shown in Figure 7(c) to 7(f). Due to the foam structure of STrGO, there will be more cavities between POE and STrGO when the composites are pressed into wafers, Figure 7(c) and 7(e). In contrast, HHrGO can be closely combined with POE as the interlamellar gap of HHrGO is less than STrGO. That is, HHrGO can completely cover the surface of POE particles with fewer interlamellar gaps, while STrGO is difficult to tightly cover the POE surface, resulting in more microcapacitors, as shown in Figure 7(d) and Figure 7(f).

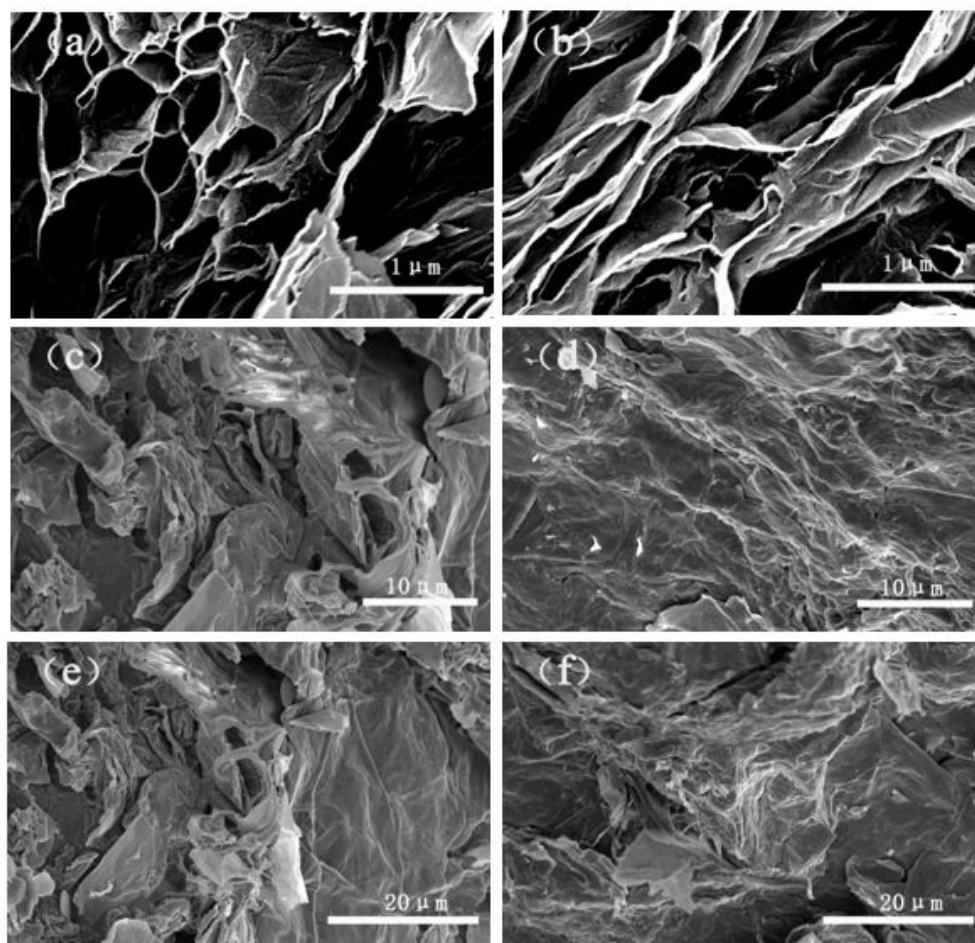


Figure 7. SEM images of STrGO(a); HHrGO(b); STrGO/POE-50(c) and (e); HHrGO/POE-50(d) and (f)

The permittivity of the composite is closely related to the change in electrical resistivity. After changing the preparation method of graphene, the ENZ property of the composites prepared with the same content of graphene shows differences. The resistivity of HHrGO/POE-40 composite is about $40 \Omega \cdot \text{cm}$ in Figure 3(b), which is smaller than that of STrGO/POE-40 shown in Figure 2(b). Similarly, the electrical resistivity of HHrGO/POE-50 is also smaller than that of STrGO/POE-50. This is because a large amount of oxygen-containing functional groups on the graphene carbon skeleton are removed by hydrazine hydrate. And the complete carbon skeleton ensures that electrons can generate delocalized transitions to a wider range, which causes the resonance frequency of HHrGO/POE lower than that of STrGO/POE. The electrical resistivity curves of STrGO and HHrGO are shown in Figure

8(a). The electrical resistivity of the HHrGO is smaller than that of the STrGO. Thus, the graphene obtained from the hydrazine hydrate reduction method possesses higher conductivity. ENZ property can be adjusted effectively by changing the preparation method of graphene. The schematic diagram of graphene and POE forming a 3D network is shown in Figure 8(b). Different porosities of HHrGO and STrGO will form conductive networks with different carrier concentrations around the POE. Figure 8(c) demonstrates the formation processes of two intrinsic metamaterials.

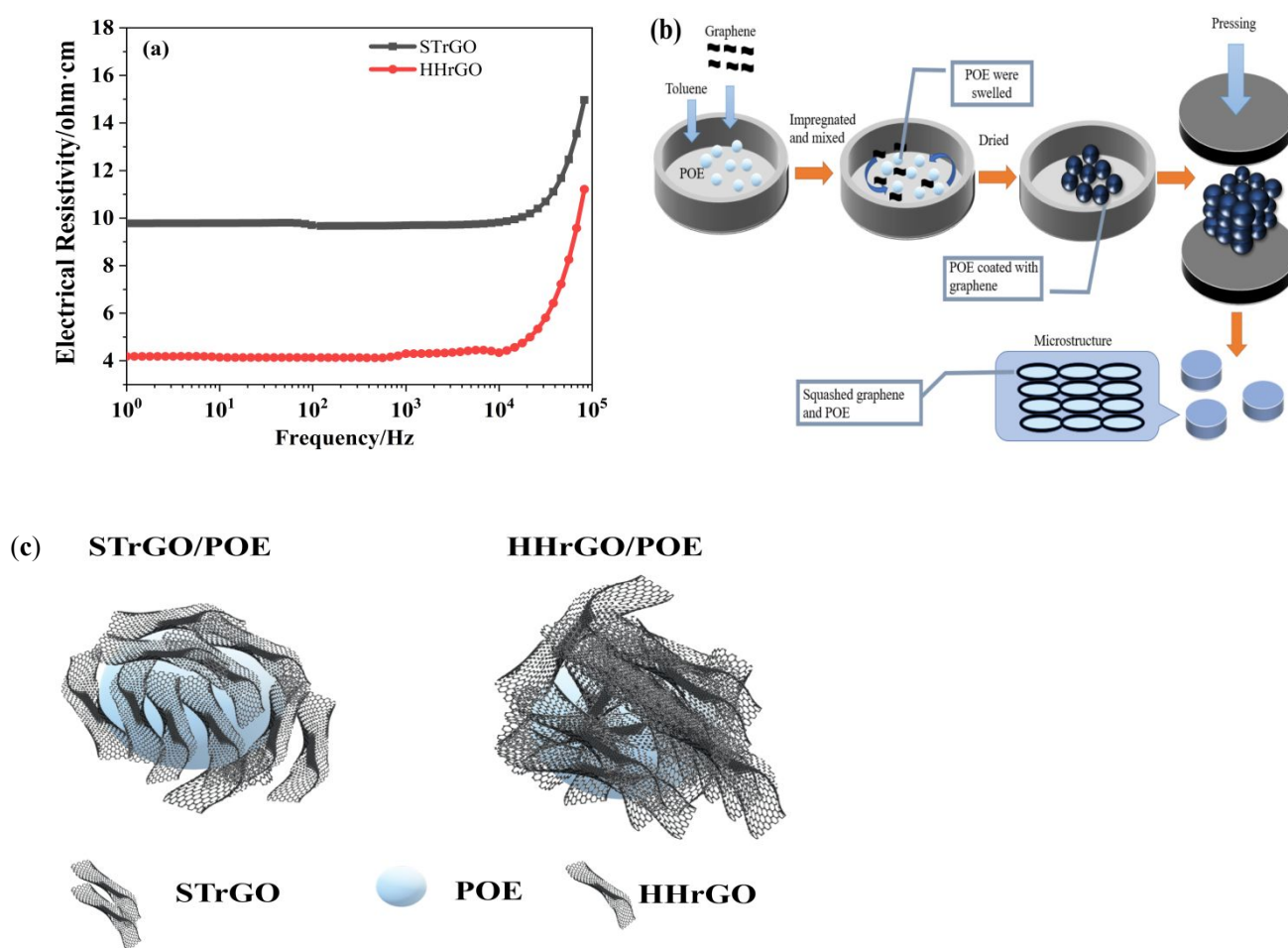


Figure 8. (a) Electrical resistivity of STrGO and HHrGO; (b) Schematic diagram of graphene (STrGO and HHrGO) and POE forming a 3D network; (c) Schematic diagram of the particle structure of HHrGO/POE and STrGO/POE

4. Conclusions

Intrinsic ENZ metamaterials based on graphene/POE metacomposites at radiofrequency were

initially constructed through reduced graphene from the solvothermal method and hydrazine hydrate reduction method, respectively. Adjustable ENZ properties in different frequency regions have been clarified via controlling graphene content and the preparation process of graphene. This result provides practical strategies to expand ENZ frequency regions and can enrich the scope of ENZ metamaterials at radiofrequency. The positive-to-negative transition in ENZ frequency region occurs with a sudden peak of the dielectric loss tangent. The near-zero permittivity is achieved with different ENZ properties in the radiofrequency region. Moreover, the peak of dielectric loss tangent during the positive-to-negative transition is a significant signal of ENZ property. The obtained ENZ property in different regions will optimize the applications like sensors and cloaks from optical frequency to lower spectra such as acoustic, water wave, and elastic wave.

Acknowledgments

This work was supported by the National Natural Science Foundation of China (51641306), Natural Science Foundation of Shanghai (16ZR1446200) and Key Basic Research Project of Shanghai (16JC1403300)

Conflict of Interest

The authors declare no conflict of interest.

References

- (1) Engheta, N. Pursuing Near-Zero Response. *Science* **2013**, *340* (6130), 286–287. <https://doi.org/10.1126/science.1235589>.
- (2) Liberal, I.; Mahmoud, A. M.; Li, Y.; Edwards, B.; Engheta, N. Photonic Doping of Epsilon-near-Zero Media. *Science* **2017**, *355* (6329), 1058–1062. <https://doi.org/10.1126/science.aal2672>.
- (3) Veselago, V. G. THE ELECTRODYNAMICS OF SUBSTANCES WITH SIMULTANEOUSLY NEGATIVE VALUES OF ϵ AND μ . *Sov. Phys. Usp.* **1968**, *10* (4), 509–514. <https://doi.org/10.1070/PU1968v010n04ABEH003699>.
- (4) Pendry, J. B.; Holden, A. J.; Stewart, W. J.; Youngs, I. Extremely Low Frequency Plasmons in Metallic Mesostructures. *Phys. Rev. Lett.* **1996**, *76* (25), 4773–4776. <https://doi.org/10.1103/PhysRevLett.76.4773>.
- (5) Pendry, J. B.; Holden, A. J.; Robbins, D. J.; Stewart, W. J. Magnetism from Conductors and Enhanced Nonlinear Phenomena. *IEEE Trans. Microwave Theory Techn.* **1999**, *47* (11), 2075–2084. <https://doi.org/10.1109/22.798002>.
- (6) Smith, D. R.; Padilla, W. J.; Vier, D. C.; Nemat-Nasser, S. C.; Schultz, S. Composite Medium with Simultaneously Negative Permeability and Permittivity. *Phys. Rev. Lett.* **2000**, *84* (18), 4184–4187. <https://doi.org/10.1103/PhysRevLett.84.4184>.
- (7) Alam, M. Z.; De Leon, I.; Boyd, R. W. Large Optical Nonlinearity of Indium Tin Oxide in Its Epsilon-near-Zero Region. *Science* **2016**, *352* (6287), 795–797. <https://doi.org/10.1126/science.aae0330>.
- (8) Javani, M. H.; Stockman, M. I. Real and Imaginary Properties of Epsilon-Near-Zero Materials. *Phys. Rev. Lett.* **2016**, *117* (10), 107404. <https://doi.org/10.1103/PhysRevLett.117.107404>.
- (9) Liu, R.; Cheng, Q.; Hand, T.; Mock, J. J.; Cui, T. J.; Cummer, S. A.; Smith, D. R. Experimental Demonstration of Electromagnetic Tunneling Through an Epsilon-Near-Zero Metamaterial at Microwave Frequencies. *Phys. Rev. Lett.* **2008**, *100* (2), 023903. <https://doi.org/10.1103/PhysRevLett.100.023903>.
- (10) Alù, A.; Silveirinha, M. G.; Salandrino, A.; Engheta, N. Epsilon-near-Zero Metamaterials and Electromagnetic Sources: Tailoring the Radiation Phase Pattern. *Phys. Rev. B* **2007**, *75* (15), 155410. <https://doi.org/10.1103/PhysRevB.75.155410>.
- (11) Jiang, X.; Lu, H.; Li, Q.; Zhou, H.; Zhang, S.; Zhang, H. Epsilon-near-Zero Medium for Optical Switches in a Monolithic Waveguide Chip at 1.9 Mm. *Nanophotonics* **2018**, *7* (11), 1835–1843. <https://doi.org/10.1515/nanoph-2018-0102>.
- (12) Lobet, M.; Majerus, B.; Henrard, L.; Lambin, P. Perfect Electromagnetic Absorption Using Graphene and Epsilon-near-Zero Metamaterials. *Phys. Rev. B* **2016**, *93* (23), 235424. <https://doi.org/10.1103/PhysRevB.93.235424>.
- (13) Silveirinha, M.; Engheta, N. Tunneling of Electromagnetic Energy through Subwavelength Channels and Bends Using ϵ -Near-Zero Materials. *Phys. Rev. Lett.* **2006**, *97* (15), 157403. <https://doi.org/10.1103/PhysRevLett.97.157403>.
- (14) Edwards, B.; Alù, A.; Young, M. E.; Silveirinha, M.; Engheta, N. Experimental Verification of Epsilon-Near-Zero Metamaterial Coupling and Energy Squeezing Using a Microwave Waveguide. *Phys. Rev. Lett.* **2008**, *100* (3), 033903. <https://doi.org/10.1103/PhysRevLett.100.033903>.
- (15) Suchowski, H.; O'Brien, K.; Wong, Z. J.; Salandrino, A.; Yin, X.; Zhang, X. Phase Mismatch-Free Nonlinear Propagation in Optical Zero-Index Materials. *Science* **2013**, *342* (6163), 1223–1226. <https://doi.org/10.1126/science.1244303>.
- (16) Jing, Y.; Xu, J.; Fang, N. X. Numerical Study of a Near-Zero-Index Acoustic Metamaterial. *Physics Letters A* **2012**, *376* (45), 2834–2837. <https://doi.org/10.1016/j.physleta.2012.08.057>.
- (17) Mocella, V.; Cabrini, S.; Chang, A. S. P.; Dardano, P.; Moretti, L.; Rendina, I.; Olynick, D.; Harteneck, B.;

- Dhuey, S. Self-Collimation of Light over Millimeter-Scale Distance in a Quasi-Zero-Average-Index Metamaterial. *Phys. Rev. Lett.* **2009**, *102* (13), 133902. <https://doi.org/10.1103/PhysRevLett.102.133902>.
- (18) Hao, J.; Yan, W.; Qiu, M. Super-Reflection and Cloaking Based on Zero Index Metamaterial. *Appl. Phys. Lett.* **2010**, *96* (10), 101109. <https://doi.org/10.1063/1.3359428>.
- (19) Maas, R.; Parsons, J.; Engheta, N.; Polman, A. Experimental Realization of an Epsilon-near-Zero Metamaterial at Visible Wavelengths. *Nature Photon* **2013**, *7* (11), 907–912. <https://doi.org/10.1038/nphoton.2013.256>.
- (20) Brown, J. Artificial Dielectrics Having Refractive Indices Less than Unity. *Proceedings of the IEE - Part IV: Institution Monographs* **1953**, *100* (5), 51–62. <https://doi.org/10.1049/pi-4.1953.0009>.
- (21) Guo, Q.; Cui, Y.; Yao, Y.; Ye, Y.; Yang, Y.; Liu, X.; Zhang, S.; Liu, X.; Qiu, J.; Hosono, H. A Solution-Processed Ultrafast Optical Switch Based on a Nanostructured Epsilon-Near-Zero Medium. *Adv. Mater.* **2017**, *29* (27), 1700754. <https://doi.org/10.1002/adma.201700754>.
- (22) Johnson, P. B.; Christy, R. W. Optical Constants of the Noble Metals. *Phys. Rev. B* **1972**, *6* (12), 4370–4379. <https://doi.org/10.1103/PhysRevB.6.4370>.
- (23) Spitzer, W. G.; Kleinman, D.; Walsh, D. Infrared Properties of Hexagonal Silicon Carbide. *Phys. Rev.* **1959**, *113* (1), 127–132. <https://doi.org/10.1103/PhysRev.113.127>.
- (24) Gholipur, R.; Khorshidi, Z.; Bahari, A. Enhanced Absorption Performance of Carbon Nanostructure Based Metamaterials and Tuning Impedance Matching Behavior by an External AC Electric Field. *ACS Appl. Mater. Interfaces* **2017**, *9* (14), 12528–12539. <https://doi.org/10.1021/acsami.7b02270>.
- (25) Wang, J.; Shi, Z.; Mao, F.; Chen, S.; Wang, X. Bilayer Polymer Metacomposites Containing Negative Permittivity Layer for New High- k Materials. *ACS Appl. Mater. Interfaces* **2017**, *9* (2), 1793–1800. <https://doi.org/10.1021/acsami.6b12786>.
- (26) Cheng, C.; Fan, R.; Wang, Z.; Shao, Q.; Guo, X.; Xie, P.; Yin, Y.; Zhang, Y.; An, L.; Lei, Y.; Ryu, J. E.; Shankar, A.; Guo, Z. Tunable and Weakly Negative Permittivity in Carbon/Silicon Nitride Composites with Different Carbonizing Temperatures. *Carbon* **2017**, *125*, 103–112. <https://doi.org/10.1016/j.carbon.2017.09.037>.
- (27) Cheng, C.; Yan, K.; Fan, R.; Qian, L.; Zhang, Z.; Sun, K.; Chen, M. Negative Permittivity Behavior in the Carbon/Silicon Nitride Composites Prepared by Impregnation-Carbonization Approach. *Carbon* **2016**, *96*, 678–684. <https://doi.org/10.1016/j.carbon.2015.10.003>.
- (28) Xie, P.; Sun, W.; Liu, Y.; Du, A.; Zhang, Z.; Wu, G.; Fan, R. Carbon Aerogels towards New Candidates for Double Negative Metamaterials of Low Density. *Carbon* **2018**, *129*, 598–606. <https://doi.org/10.1016/j.carbon.2017.12.009>.
- (29) Gu, H.; Xu, X.; Dong, M.; Xie, P.; Shao, Q.; Fan, R.; Liu, C.; Wu, S.; Wei, R.; Guo, Z. Carbon Nanospheres Induced High Negative Permittivity in Nanosilver-Polydopamine Metacomposites. *Carbon* **2019**, *147*, 550–558. <https://doi.org/10.1016/j.carbon.2019.03.028>.
- (30) Yao, X.; Kou, X.; Qiu, J. Multi-Walled Carbon Nanotubes/Polyaniline Composites with Negative Permittivity and Negative Permeability. *Carbon* **2016**, *107*, 261–267. <https://doi.org/10.1016/j.carbon.2016.05.055>.
- (31) Luo, H.; Qiu, J. Carbon Nanotubes / Epoxy Resin Metacomposites with Adjustable Radio-Frequency Negative Permittivity and Low Dielectric Loss. *Ceramics International* **2019**, *45* (1), 843–848. <https://doi.org/10.1016/j.ceramint.2018.09.253>.
- (32) Li, B.; Sui, G.; Zhong, W.-H. Single Negative Metamaterials in Unstructured Polymer Nanocomposites Toward Selectable and Controllable Negative Permittivity. *Adv. Mater.* **2009**, *21* (41), 4176–4180. <https://doi.org/10.1002/adma.200900653>.

- (33) Zhu, J.; Zhang, X.; Haldolaarachchige, N.; Wang, Q.; Luo, Z.; Ryu, J.; Young, D. P.; Wei, S.; Guo, Z. Polypyrrole Metacomposites with Different Carbon Nanostructures. *J. Mater. Chem.* **2012**, 22 (11), 4996. <https://doi.org/10.1039/c2jm14020a>.
- (34) Cheng, C.; Fan, R.; Ren, Y.; Ding, T.; Qian, L.; Guo, J.; Li, X.; An, L.; Lei, Y.; Yin, Y.; Guo, Z. Radio Frequency Negative Permittivity in Random Carbon Nanotubes/Alumina Nanocomposites. *Nanoscale* **2017**, 9 (18), 5779–5787. <https://doi.org/10.1039/C7NR01516J>.
- (35) Luo, H.; Qiu, J. Carbon Nanotube/Polyolefin Elastomer Metacomposites with Adjustable Radio-Frequency Negative Permittivity and Negative Permeability. *Adv. Electron. Mater.* **2019**, 5 (6), 1900011. <https://doi.org/10.1002/aelm.201900011>.
- (36) Li, D.; Müller, M. B.; Gilje, S.; Kaner, R. B.; Wallace, G. G. Processable Aqueous Dispersions of Graphene Nanosheets. *Nature Nanotech* **2008**, 3 (2), 101–105. <https://doi.org/10.1038/nnano.2007.451>.
- (37) Jin, H.; Bu, Y.; Li, J.; Liu, J.; Fen, X.; Dai, L.; Wang, J.; Lu, J.; Wang, S. Strong Graphene 3D Assemblies with High Elastic Recovery and Hardness. *Adv. Mater.* **2018**, 30 (36), 1707424. <https://doi.org/10.1002/adma.201707424>.
- (38) Balci, O.; Kakenov, N.; Karademir, E.; Balci, S.; Cakmakyapan, S.; Polat, E. O.; Caglayan, H.; Özbay, E.; Kocabas, C. Electrically Switchable Metadevices via Graphene. *Sci. Adv.* **2018**, 4 (1), eaao1749. <https://doi.org/10.1126/sciadv.aao1749>.
- (39) Sun, H.; Xu, Z.; Gao, C. Multifunctional, Ultra-Flyweight, Synergistically Assembled Carbon Aerogels. *Adv. Mater.* **2013**, 25 (18), 2554–2560. <https://doi.org/10.1002/adma.201204576>.
- (40) Alù, A.; Engheta, N. Dielectric Sensing in ϵ -near-Zero Narrow Waveguide Channels. *Phys. Rev. B* **2008**, 78 (4), 045102. <https://doi.org/10.1103/PhysRevB.78.045102>.
- (41) Lobato-Morales, H.; Corona-Chavez, A.; Olvera-Cervantes, J. L. Planar Sensors for RFID Wireless Complex-Dielectric-Permittivity Sensing of Liquids. In *2013 IEEE MTT-S International Microwave Symposium Digest (MTT)*; IEEE: Seattle, WA, USA, 2013; pp 1–3. <https://doi.org/10.1109/MWSYM.2013.6697735>.
- (42) Li, Y.; Zhu, K.-J.; Peng, Y.-G.; Li, W.; Yang, T.; Xu, H.-X.; Chen, H.; Zhu, X.-F.; Fan, S.; Qiu, C.-W. Thermal Meta-Device in Analogue of Zero-Index Photonics. *Nature Mater* **2019**, 18 (1), 48–54. <https://doi.org/10.1038/s41563-018-0239-6>.
- (43) Shi, Z.; Fan, R.; Zhang, Z.; Qian, L.; Gao, M.; Zhang, M.; Zheng, L.; Zhang, X.; Yin, L. Random Composites of Nickel Networks Supported by Porous Alumina Toward Double Negative Materials. *Adv. Mater.* **2012**, 24 (17), 2349–2352. <https://doi.org/10.1002/adma.201200157>.
- (44) Estevez, D.; Qin, F.; Luo, Y.; Quan, L.; Mai, Y.-W.; Panina, L.; Peng, H.-X. Tunable Negative Permittivity in Nano-Carbon Coated Magnetic Microwire Polymer Metacomposites. *Composites Science and Technology* **2019**, 171, 206–217. <https://doi.org/10.1016/j.compscitech.2018.12.016>.
- (45) Yao, X.; Kou, X.; Qiu, J.; Moloney, M. The Generation Mechanism of Negative Permittivity in Multi-Walled Carbon Nanotubes/Polyaniline Composites. *RSC Adv.* **2016**, 6 (42), 35378–35386. <https://doi.org/10.1039/C6RA03956A>.
- (46) Gu, H.; Guo, J.; He, Q.; Jiang, Y.; Huang, Y.; Haldolaarachchige, N.; Luo, Z.; Young, D. P.; Wei, S.; Guo, Z. Magnetoresistive Polyaniline/Multi-Walled Carbon Nanotube Nanocomposites with Negative Permittivity. *Nanoscale* **2014**, 6 (1), 181–189. <https://doi.org/10.1039/C3NR04152B>.

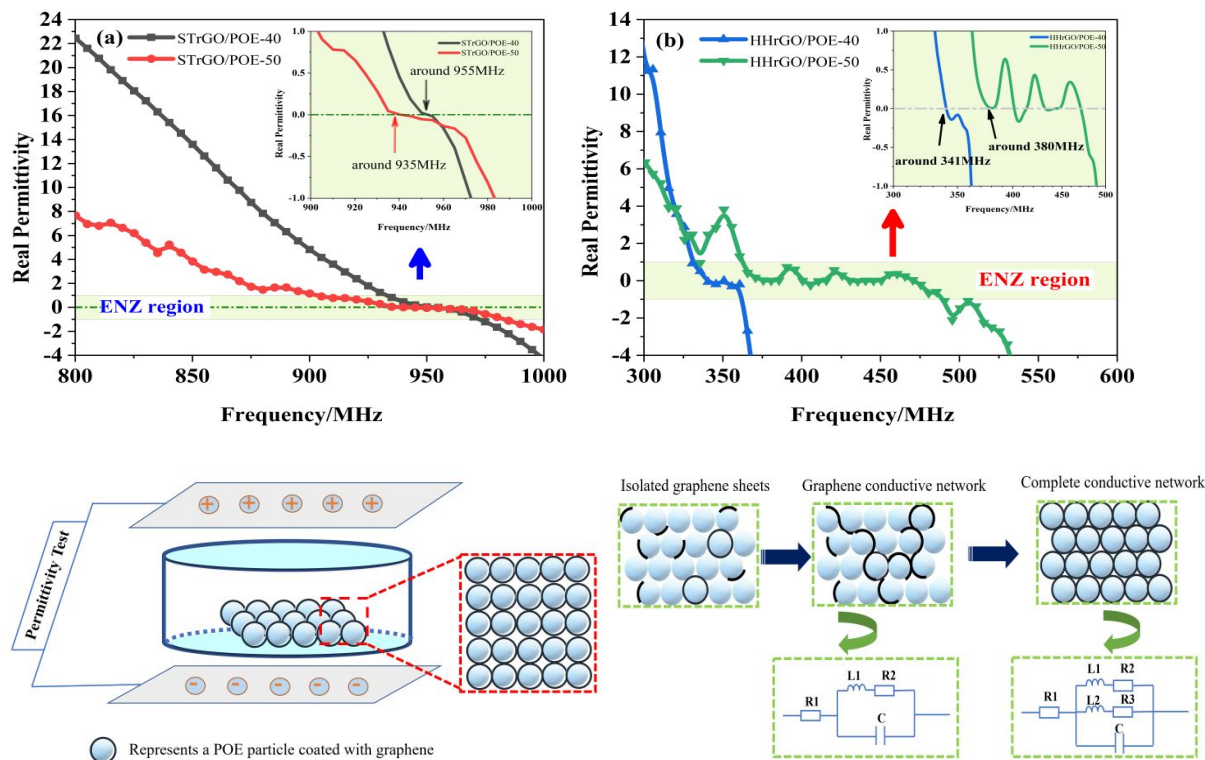


Figure 1. ENZ properties realized in intrinsic metamaterials at radiofrequency (a) STrGO/POE metamaterials; (b) HHrGO/POE metamaterials; (c) Schematic of the sample in the test system; (d) Schematic of the conductive networks at the positive-to-negative transition frequency

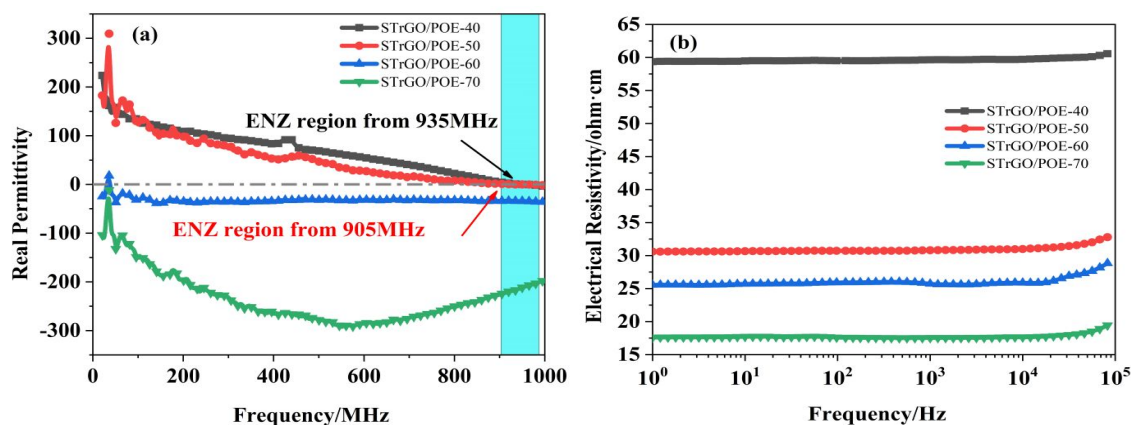


Figure 2. (a) Real permittivity of STrGO/POE metamaterials as a function of frequency; (b) Electrical resistivity of STrGO/POE metamaterials as a function of frequency

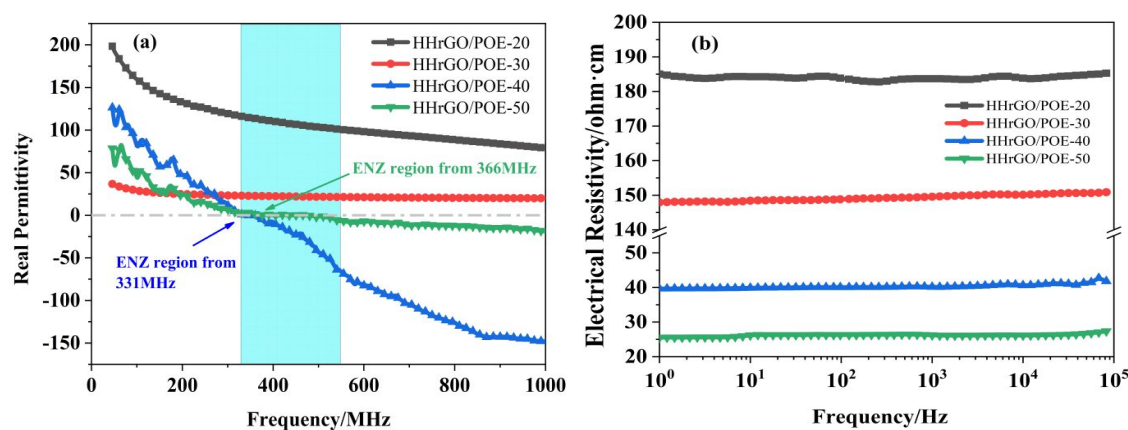


Figure 3. (a) Real permittivity of HHrGO/POE metamaterials as a function of frequency; (b) Electrical resistivity of HHrGO/POE metamaterials as a function of frequency

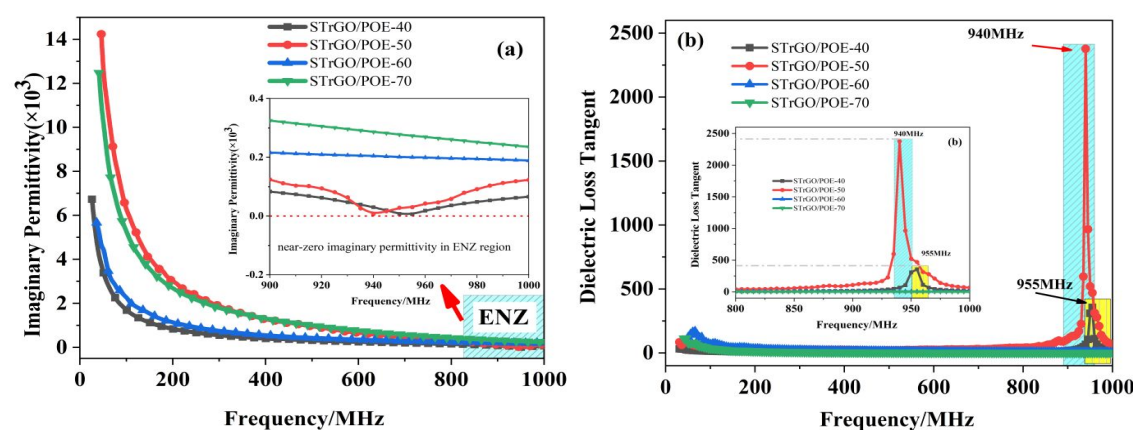


Figure 4. (a) Imaginary permittivity and (b) Dielectric loss tangent ($\tan \delta$) of STrGO/POE metamaterials under different frequency

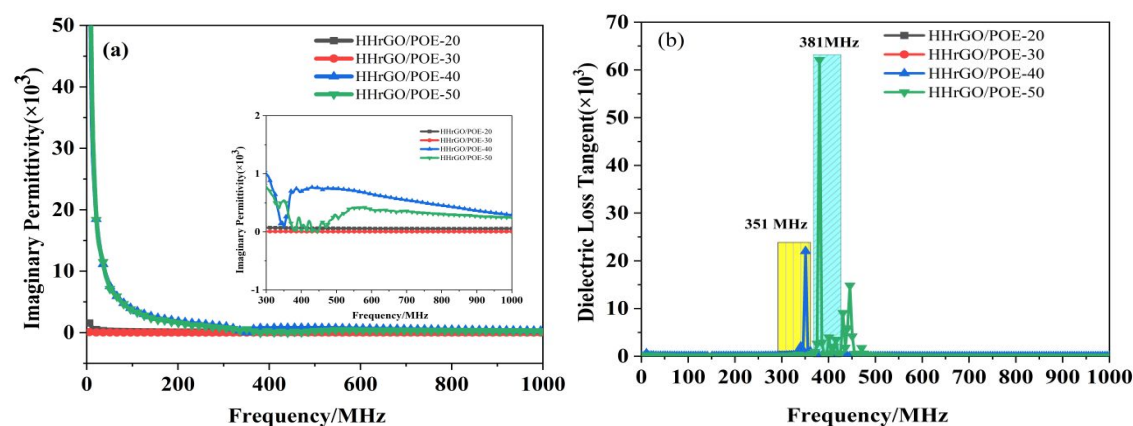


Figure 5. (a) Imaginary permittivity and (b) Dielectric loss tangent ($\tan \delta$) of HHrGO/POE metamaterials under different frequency

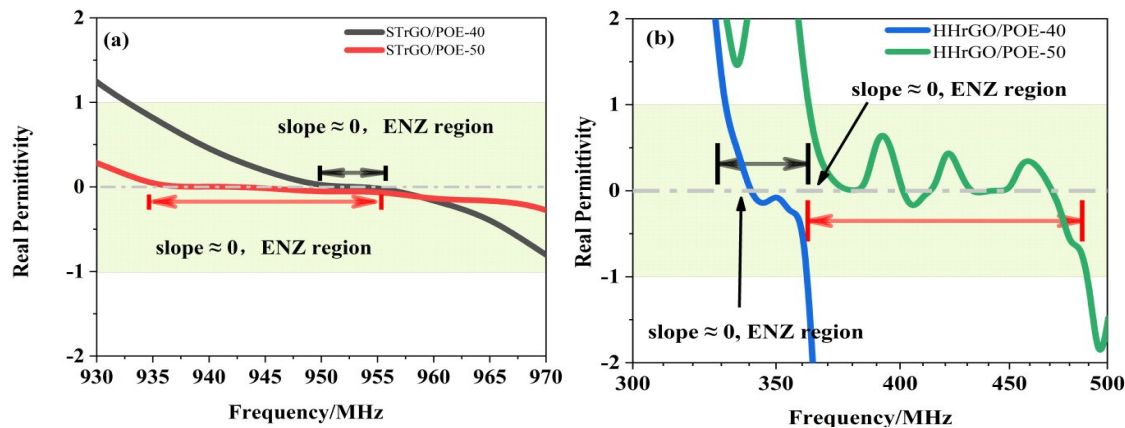


Figure 6. Enlarged views of the frequency region from positive to negative in ENZ metamaterials: (a) STrGO/POE metamaterials; (b) HHrGO/POE-40 metamaterials

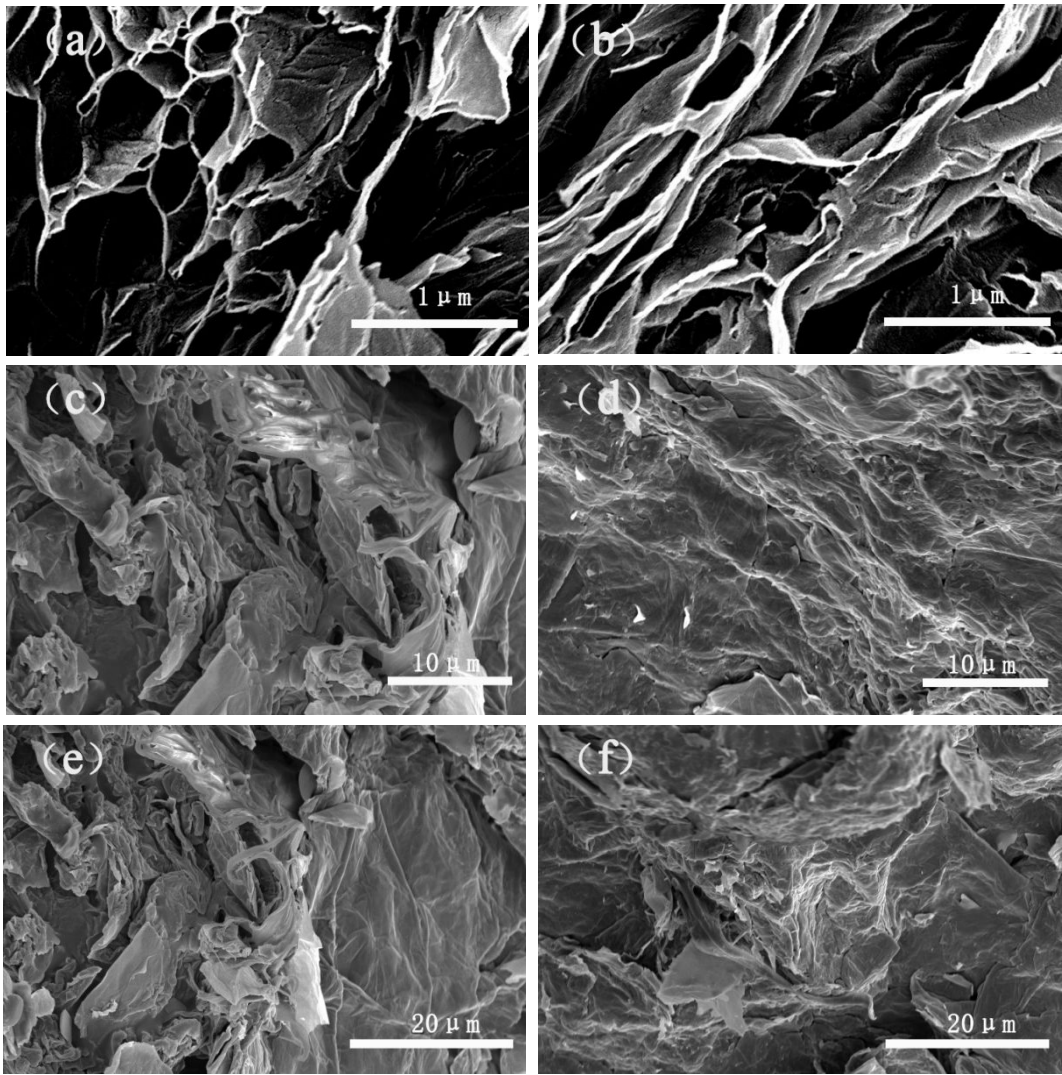


Figure 7. SEM images of STrGO(a); HHrGO(b); STrGO/POE-50(c) and (e); HHrGO/POE-50(d) and (f)

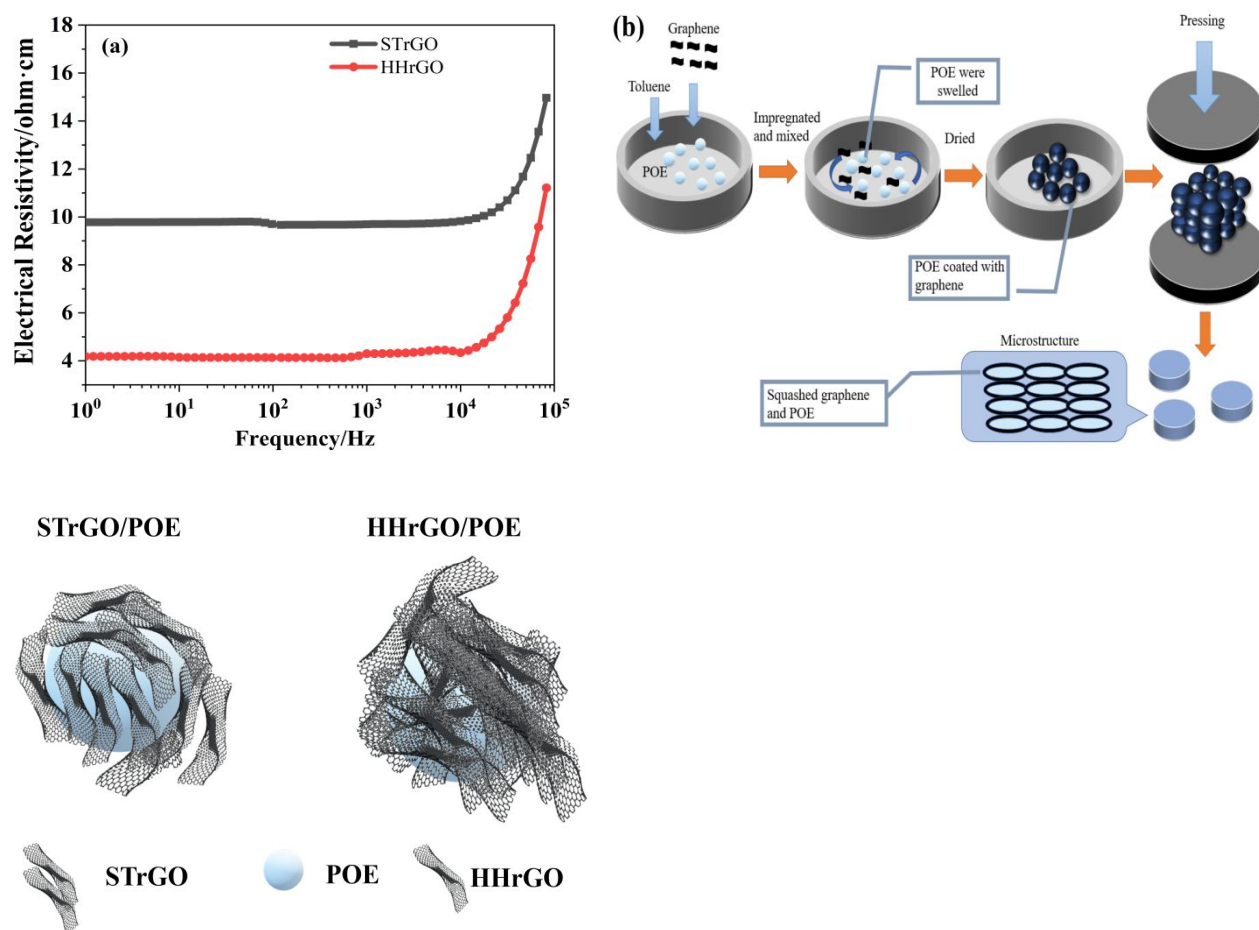


Figure 8. (a) Electrical resistivity of STrGO and HHrGO; (b) Schematic diagram of graphene (STrGO and HHrGO) and POE forming a 3D network; (c) Schematic diagram of the particle structure of HHrGO/POE and STrGO/POE

Graphene/POE intrinsic ENZ metamaterials are initially prepared with adjustable broadband ENZ properties. The ENZ properties can be regulated by adjusting the graphene content and changing the preparation methods of graphene.

Keyword Epsilon-near-zero, intrinsic metamaterials, graphene, adjustability, radiofrequency

Ji Dai, Hongchun Luo, Mark Moloney, Jun Qiu*

Adjustable Graphene/Polyolefin Elastomer Epsilon-near-zero Metamaterials at Radiofrequency Range

